Soft Matter

Cite this: *Soft Matter*, 2012, **8**, 7937

www.rsc.org/softmatter

PAPER

Phase structural formation and oscillation in polystyrene-*block*-polydimethylsiloxane thin films

I-Fan Hsieh,[a] Hao-Jan Sun,[a] Qiang Fu,*[b] Bernard Lotz,[c] Kevin A. Cavicchi[d] and Stephen Z. D. Cheng*[a]

Received 30th March 2012, Accepted 29th May 2012
DOI: 10.1039/c2sm25749a

The solvent-induced spherical structure in a polystyrene-*block*-polydimethylsiloxane (PS-*b*-PDMS) block copolymer was obtained and stabilized by preparing both the bulk and thin films from propylene glycol methyl ether acetate (PGMEA) solutions. The diblock copolymer possessed a total molecular weight of 42 kDa with a PS volume fraction of 72.2%, and it formed a cylindrical phase structure in the equilibrium bulk state. During thermal annealing, only changes in the sphere size and packing rearrangement were found. In contrast, a unique structure evolution route was observed during solvent treatments. Under a controlled vapour of a PS selective solvent, an oscillation of the structural transition between spheres and cylinders was observed in the thin films. The kinetics of this oscillation of structural transition was found to be closely related to the solvent vapour concentration and film thickness. This experiment revealed a unique ordering pathway towards the equilibrium structure in the thin film for this strongly segregated PS-*b*-PDMS diblock copolymer.

Introduction

Block copolymers are well-known to self-assemble into periodic ordered structures. This has generated intense interest in their use to pattern surfaces in the form of nano-structured thin films for various applications including lithographic masks, separation membranes, inorganic nano-materials templating, and photovoltaics.[1–6] One key factor to the success of this approach is developing processes to repeatedly produce films with the desired morphology, long-range order and domain orientation. Solvents are widely used to process block copolymer films, both through the initial casting to obtain a substrate supported thin film and additional controlled solvent swelling, also referred to as solvent annealing.[7] The role of a solvent in the development of the morphology is complex as it influences both the kinetics and thermodynamics of the system through plasticization; mediating interactions between the blocks; the substrate–polymer and air–polymer interfaces; and/or selectively swelling the domains shifting the spontaneous curvature of the system.[8–10]

In the simplest case the solvent plasticizes the glassy blocks and mediates the enthalpic interactions, reducing the effective interaction parameter of the system (χ_{eff}) to speed up the chain dynamics and allow longer-range order to develop through the annealing out of defects.[10] In the case where the solvent is selective for one of the blocks an order–order transition may also take place during annealing resulting from the preferential swelling of one block increasing its effective volume fraction and shifting the spontaneous curvature of the system.[11–13] To a first approximation, these combined effects of the interactions and volume fraction on the equilibrium morphology are captured by the idea of phase trajectories on the melt phase diagram.[8] For a neutral solvent, swelling lowers χ_{eff} resulting in the vertical trajectory through phase space towards disorder with increasing solvent concentration. For a selective solvent both χ_{eff} and the volume fraction shift result in a diagonal to horizontal trajectory through phase space, with the deviation from the neutral solvent condition depending on the level of solvent selectivity. Therefore, after swelling to a constant solvent concentration the system will order to adopt the equilibrium morphology. While similar to the bulk, the morphological behaviour can be further complicated in thin films due to the effects of solvent substrate–polymer and air–polymer interactions, which can drive surface reconstructions.[9,14,15]

One recent investigation by Wang *et al.* indicates that ordering of solvent swollen systems is more complicated under certain situations where cyclic ordering through order–order transitions (OOTs) occurs and may provide an alternative thermodynamic pathway to refine the morphology and obtain long-range order.[16] The ordering of solvent swollen poly(styrene-*block*-ethylene-*co*-butylene-*block*-styrene) (PS-*b*-PEB-*b*-PS) triblock copolymer thin films was characterized by scanning force microscopy. The films were cast from xylene to obtain poorly ordered, short

[a]*Department of Polymer Science, College of Polymer Science and Polymer Engineering, The University of Akron, Akron, Ohio 44325-3909, USA. E-mail: scheng@uakron.edu*
[b]*College of Polymer Science and Engineer, State Key Laboratory of Polymer Materials Engineering, Sichuan University, Chengdu 610065, Sichuan, China*
[c]*Institut Charles Sadron (CNRS-Université de Strasbourg) F-67034, Strasbourg, France*
[d]*Department of Polymer Engineering, College of Polymer Science and Polymer Engineering, The University of Akron, Akron, Ohio 44325-0301, USA*

aspect ratio cylinders. Upon annealing with cyclohexane, a solvent selective towards the majority PEB block, a transition to a hexagonally packed sphere morphology was observed. Interestingly, a cyclic transition between cylinders and spheres was seen when annealing the same sample for longer times, or annealing multiple samples for different times. This cycling was a surprising result. Thermally induced OOTs between body-centred cubic spheres and hexagonally packed cylinders have been observed in bulk and solvent swollen melts.[17–25] However, *in situ* rheological and scattering measurements have not shown evidence of cyclic transitions. On the other hand, recent *in situ* characterization of the morphology development during thermal annealing of block copolymer thin films indicates that local OOTs occur as a mechanism to anneal out defects.[26,27] Also, a transient cylinder to sphere transition is found to occur in the reorientation of parallel cylinders to perpendicular cylinders under applied electric fields.[28,29] As solvent introduces an additional degree of freedom in the system it could lower the thermodynamic barriers to phase coexistence and cyclic transitions.

It should be noted that a cyclic transition from spheres to cylinders to spheres has also been observed in solvent swollen poly(styrene-*block*-4-vinylpyridine) thin films.[30,31] However, this was attributed to spin-coating conditions, which resulted in an initially kinetically trapped sphere phase, which when swollen with solvent resulted in a phase trajectory that passed through an equilibrium cylinder phase during swelling before transitioning back to spheres. Transient swelling effects could contribute to the results at short times, but in the case of the investigation by Wang *et al.* cyclic transitions are observed over the course of hours, which should be considerably longer than the time required to reach swelling equilibrium of the thin film.

From the fundamental viewpoint, a thorough understanding of the mechanism and kinetics of the ordering processes is important for the practical control of block copolymer morphology, and further can make the block copolymer more adaptable for nanotechnological applications. This study reports the phase structural evolutions of thin films of a polystyrene-*block*-polydimethylsiloxane (PS-*b*-PDMS) block copolymer during thermal annealing and solvent treatment investigated *via* time-resolved transmission electron microscopy (TEM). By using selective solvents an order–order transition from spheres to parallel cylinders is observed. Most notably, oscillations between ordered sphere and cylinder phases were observed before the stabilization of the cylinder phase. This shows similarities to the previously observed oscillating cylinder to sphere transition by Wang *et al.*[32] The dependence of the structural evolution on the film thickness and solvent choice is also discussed.

Experimental

Materials

A PS-*b*-PDMS block copolymer ($M_{n,PS} = 31$ kDa, $M_{n,PDMS} = 11$ kDa, and $M_w/M_n = 1.10$) was purchased from Polymer Source Inc. and used as received.

Film preparation and solvent treatment

Thin film samples were prepared by spin coating or drop casting from propylene glycol methyl ether acetate (PGMEA) solutions, which is a solvent that is commonly used in the microelectronic industry, especially for lithography, on carbon coated mica. The film thickness was controlled by the solution concentration and spin coating rate. The solution concentration used ranged from 1 wt% to 2 wt% and the spin coating rate ranged from 2000 rpm to 6000 rpm. Solvent treatment was done by using an apparatus that consisted of two nitrogen lines: one goes through a solvent reservoir and another is pure nitrogen. The solvent concentration during the treatment is controlled by varying the flow rates of pure and solvent infused nitrogen.

Characterization

A bulk sample was cast from PGMEA solution and examined by small angle X-ray scattering (SAXS). The SAXS was performed at beamline 23A1 at the National Synchrotron Radiation Research Center (NSRRC) in Hsin-Chu, Taiwan. The thin film thickness was measured by an ellipsometer (J. A. Woollam Co., Inc., VB-400 VASE). The local film thickness (T_1, T_2, …layer) was measured by AFM using a scratch method to trace the same layer in different samples. The thin films were floated by immersing a carbon-coated mica substrate into water surface and the film was picked up by a TEM copper gird. The morphologies of PS-*b*-PDMS thin films were examined by a TEM (JEOL JEM-1230) operated at 120 kV in bright field. The TEM images of the thin film samples were captured at several spots (>40) that were representative of the whole sample.

Results and discussion

The sample used was a PS-*b*-PDMS block copolymer with a total molecular weight of 42 kDa and a volume fraction of the PS blocks of $f_{PS} = 72.2\%$. This block copolymer shows a thermodynamic equilibrium structure of hexagonal packed cylinders in the bulk state. The Flory–Huggins χ parameter for PS-*b*-PDMS at room temperature is much larger than other commonly used block copolymers.[33] For example, its χ value (0.26 at 25 °C)[34] is about 3 times larger than the χ parameter between PS and polyethylene (0.08 at 25 °C)[35] that is a traditionally viewed diblock copolymer with a strong phase separation. Due to the larger χN values in the PS-*b*-PDMS system, it is possible to obtain morphologies with either much smaller periodicities and/or sharper interfaces compared to other commonly used block copolymer systems. Another advantage of the PS-*b*-PDMS system is that PS and PDMS blocks possess large etch contrasts under oxygen-plasma[36,37] or ultraviolet (UV) exposure with ozone treatment.[38] After UV/ozone or oxygen-plasma treatment, PDMS can readily form silicon oxide and PS can be degraded to become monomers or small segments. These advantages make PS-*b*-PDMS a useful candidate for nano-imprint and nano-lithography.[39]

As-spun and thermally annealed morphology

Fig. 1a shows the bright-field TEM image for a PS-*b*-PDMS drop cast thin film from PGMEA solution. By taking advantage of the high electron density contrast between the PDMS and PS blocks, we can observe the thin film morphology under TEM without a staining procedure. As shown in this figure, the PDMS blocks form round domains with hexagonal packing in the PS block

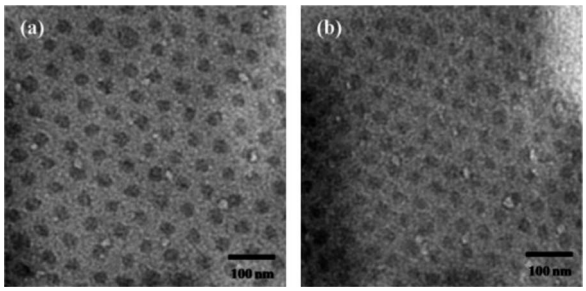

Fig. 1 (a) PS-*b*-PDMS–PGMEA solution drop cast film and (b) TEM tilted image (tilted angle 40°).

matrix, suggesting that the PDMS blocks assemble as either cylinders perpendicular to the substrate or spheres in this drop-cast film. To further identify the structure, a tilted TEM technique was employed. During tilting, the shape of the PDMS domains does not change, yet the distance between the neighboring PDMS domains decreases from 17 nm to 13 nm after a tilt of 40°, as shown in Fig. 1b. This observation indicates that the PDMS domains in the film are spherical rather than cylindrical. Here it should be noted that a hexagonally packed cylinder is the thermodynamic equilibrium structure for this sample in the bulk state.

An important question is whether the formation of a spherical structure in the thin film is due to the constraints of the film thickness or solvent effects during the casting process. To answer this question, we conducted a parallel study of the PS-*b*-PDMS/PGMEA in the bulk by casting thicker films with a thickness in the micrometer scale. The PS-*b*-PDMS bulk sample also exhibits a different phase structure deviating from its equilibrium structure of hexagonally packed cylinders. Fig. 2 depicts a SAXS profile of the PS-*b*-PDMS/PGMEA bulk sample (solid line). The scattering peak arising from the inter-micro-domain interference of the scattered field is marked by a solid arrow. This SAXS profile only possesses one scattering peak located at $q \sim 0.2$ nm^{-1} indicating that the PS-*b*-PDMS/PGMEA bulk sample forms a micro-phase separated morphology which has an inter-micro-domain spacing around 31 nm. The SAXS profile does not show any higher order scattering peaks in the q region studied, indicating that the PDMS domains do not form a long-range ordered structure in this PS-*b*-PDMS/PGMEA bulk sample. Two dotted arrows indicate the peaks arising from the form factor scattering (denoted by "$i = n$" with $n = 1, 2, \ldots$) from isolated spherical domains. The average radius of PDMS spheres ($\langle R \rangle$) deduced from the positions of the form factor maxima is 13.9 nm. The red dashed line signifies the form factor profile of spheres calculated by assuming $\langle R \rangle = 13.9$ nm and the standard deviation of R, $\sigma_R = 1.5$ nm and the thickness of the diffuse phase boundary $\sigma = 1$ nm.[40] The calculated results show a good agreement with experimental data. Since the spherical structure is observed in the bulk sample, we can conclude that formation of the spherical structure is mainly driven by solvent effects during the formation process.

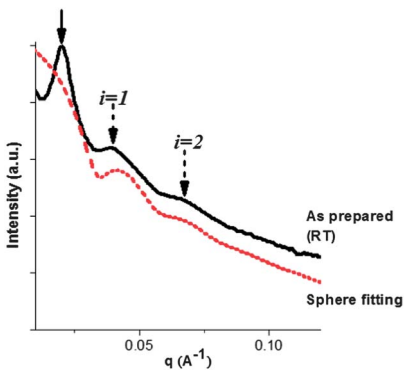

Fig. 2 SAXS data for the PS-*b*-PDMS bulk sample drop cast from PGMEA solution. Black line: experimental data; red line: fitting curve.

The solubility parameter δ_{PGMEA} for PGMEA is ~18.2 (J cm^{-3})$^{1/2}$. Therefore, it is a better solvent for PS ($\delta_{PS} \sim 18.6$ (J cm^{-3})$^{1/2}$) than PDMS (($\delta_{PDMS} \sim 15.4$ (J cm^{-3})$^{1/2}$) and preferentially swells the PS blocks. We speculate that this drives the formation of the sphere structure during casting.[8,41] In the solvent evaporation, the PS volume fraction gradually decreases toward its original bulk state composition; meanwhile, the PS glass transition temperature gradually increases as the solvent concentration decreases. In the PS-*b*-PDMS/PGMEA system, the phase structure is frozen when the solvent swollen PS glass transition temperature (T_g^{PS}) reaches ambient temperature.[42] This vitrification prevents the system from adopting the thermodynamic equilibrium cylinder structure. Therefore, the metastable PDMS sphere structure can be found in both the thin film and the bulk states. After heating the system to temperatures above the T_g^{PS}, the stability of the spherical structure depends upon the kinetic barrier for the transition from the spheres to cylinders. If the transition barrier is not high, the thermodynamic equilibrium cylindrical structure is expected to be reached. On the other hand, when this barrier is very high, the spherical structure may be retained and thus, this structure can be trapped in a metastable state.

Fig. 3a and b show two bright-field TEM images of micro-phase separated structures of spin coated films with a thickness of ~56 nm before (Fig. 3a) and after (Fig. 3b) thermal annealing. The phase structure of the as-spun film is shown in Fig. 3a in which the PDMS spheres do not exhibit a long-range ordered packing. In a thermal annealing process, instead of transferring to its thermodynamic equilibrium cylindrical structure, the PS-*b*-PDMS thin film remains as spheres as shown in Fig. 3b. Both the spacing between the neighboring spheres and the sphere diameter increase after being annealed at 180 °C for 1 day. This retained spherical structure can be confirmed by a tilted TEM bright image as shown in Fig. 3c. The IR spectrum (not shown) confirms that after thermal annealing, there is very little residual solvent remained in the thin film sample, and the retention of the

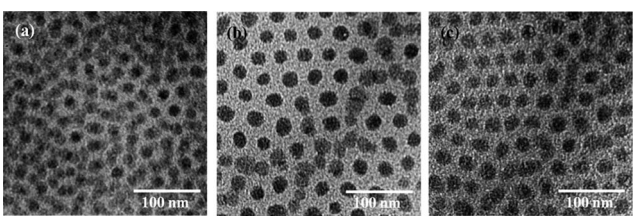

Fig. 3 (a) PS-*b*-PDMS–PGMEA solution spin coated film, (b) after 180 °C annealed for 24 hours. (c) Tilted TEM for (b) (tilted angle 40°).

spherical structure is thus no longer due to the existence of solvent. The similar phenomenon also can be found in the bulk sample. Fig. 4 shows SAXS profiles of the PS-*b*-PDMS/PGMEA bulk sample before (black line) and after thermal annealing (red line). The SAXS profile does not change its shape and only the inter-micro-domain spacing increases after thermal annealing. These results suggest that a locally trapped metastable state possesses a high barrier for these solvent-induced PDMS spheres to transition to cylinders. The main reason for retaining this metastable state is due to the fact that the strong χ parameter between the PS and PDMS blocks constructs a high enthalpic barrier for the local mixing of the PS and PDMS blocks that would be required for a transformation, such as fusion, even though the thermal annealing was carried out significantly above the T_g^{PS} of the PS blocks. The energy provided by the thermal annealing thus only allows for local rearrangements of the existing PDMS spheres.

Solvent annealed morphology

In contrast to the thermal annealing, solvent treatment provides a more efficient pathway to investigate the structural transition behavior in the PS-*b*-PDMS thin films. The existence of the solvent vapor not only acts as a plasticizer that enhances chain mobility, but also screens the interaction between PS and PDMS blocks and results in the decreases of the effective χ value between PS and PDMS in the PS-*b*-PDMS thin films. The films were treated by solvent vapor by flowing solvent infused air through a closed chamber, as has been previously practiced.[43,44] In the first experiment a PS-*b*-PDMS thin film was treated with benzene vapor. Note that benzene ($\delta_{benzene} \sim 18.8$ (J cm^{-3})$^{1/2}$) is a moderately selective solvent for the PS blocks to swell the PS matrix. During the solvent treatment, the films develop terraces with thicknesses that are thinner or thicker than the original film thickness, with a well-defined phase structure formed within each terrace. According to the local film thickness, the terraces are designated as T_1, T_2 and T_3 layers as thickness increases, and the structural transitions within each layer are monitored as the solvent treatment time increases.

Fig. 5 shows two sets of bright-field TEM images of the PS-*b*-PDMS thin film with an original thickness of ~30 nm treated under controlled benzene solvent vapor pressure. The thinner T_1 layer remains as a spherical structure after being treated for 2 hours (Fig. 5a). It then transfers partially to cylinders which are parallel to the film substrate after 3 hours (Fig. 5b) as would be expected for a transition to the thermodynamic equilibrium structure. However, after a prolonged treatment time of 6 hours, the partially formed cylinders transfer completely back to spheres (Fig. 5c). As the treatment time extends to 10 hours, the spheres again partially transfer to parallel cylinders (Fig. 5d). Finally after the treatment of 14 hours, a transition to entirely parallel cylinders is obtained with classical Frank defects commonly observed in liquid crystals and diblock copolymers (Fig. 5e).[45,46] Therefore, it is apparent that the structural transition between the spheres and cylinders oscillates within the solvent treatment time studied. Similar observations are found within the terrace of the T_2 layer as shown in Fig. 5f–j. The initial spheres partially transfer to cylinders at a treatment time of 2 hours (Fig. 5f), and the cylinders oscillate back to spheres at a treatment time of 3 hours (Fig. 5g). The spheres are stable for a while and then partially transfer to cylinders again at a treatment time of 6 hours (Fig. 5h). Further prolonging the time for the solvent treatment, the cylindrical structure gradually develops back (Fig. 5i and j). During the benzene solvent treatment, an oscillation of the structural transition between the spheres and cylinders is thus observed as a general phenomenon in both terraces of T_1 and T_2 layer thicknesses.

This unique structural transition behavior is not restricted to a specific film thickness. Fig. 6 shows three sets of the structural transition behaviors for a thin film with an initial thickness of ~56 nm during controlled benzene solvent vapor treatment. In this relatively thicker film, a more complex structure formation can be apparently observed due to the overlapping of multiple layers of structures in the bright-field TEM images. If we look at the structural transition in the terraces of different thicknesses during the solvent vapor treatment, we can still find the structural oscillation between spheres and cylinders within each layer. However, it should be noted that although the thin film thickness does not affect the mechanism of the structural transition, it alters the kinetics of the structural transition. Namely, the spherical structure in the terraces of the T_2 film region is relatively easier than that of the thicker T_3 film region to relax to its thermodynamic equilibrium cylindrical structure. For example, after the benzene solvent vapor treatment of 20 hours in the T_3 terrace, the thermodynamic equilibrium state of cylindrical structure becomes permanent (Fig. 6a–f). Within the T_2 terrace before the benzene solvent vapor treatment of 12 hours, the

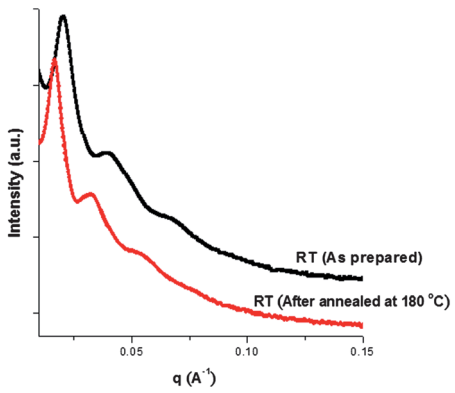

Fig. 4 SAXS data for the PS-*b*-PDMS bulk sample drop cast from PGMEA solution. Black line: as prepared sample; red line: sample after thermal annealing.

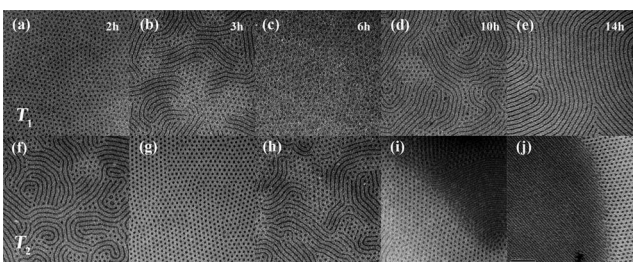

Fig. 5 Thin film structural transition during benzene solvent annealing (original film thickness of ~30 nm). Each image is about 1.2 μm × 1.2 μm.

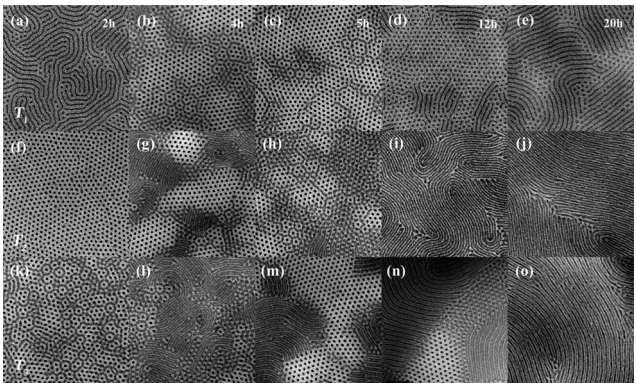

Fig. 6 Thin film structural transition during benzene solvent annealing (original film thickness of ~56 nm). Each image is about 1 μm × 1 μm.

oscillating structural transitions take place (Fig. 6f–h). After the solvent vapor treatment of 12 hours the cylindrical structure becomes thermodynamically stable (Fig. 6i), and no further oscillating structural transition can be observed even with a prolonged solvent vapor treatment time studied (Fig. 6j). In contrast, we observed the oscillating structural transition between spheres and cylinders in the thinner T_1 layer even up to solvent vapor treatment times of 24 hours (Fig. 6k–o). This reflects not only the film thickness effect and thus, the thin film constraint, but also preference of the film thickness on the kinetics of oscillation of the structural formation to achieve the final thermodynamic equilibrium state.

Further examining the TEM observations shown in Fig. 6, some apparent polygonal phase structures are found in the thicker films during the benzene vapor treatment: for example, this polygonal phase structure that appears in the samples in the T_3 layer after 2 hours (Fig. 6k) and in the T_1 layer at 4 and 5 hours (Fig. 6b and c) under the vapor treatment. The formation of this type of structure may be associated with the relative packing of the sphere domains in multiple-layers. This polygonal phase structure is composed of two parts: one is the spheres with darker PDMS domains that pack into the hexagonal packing. Fig. 7a shows a tilted TEM image for this structure, and we find that after the sample was tilted 50°, one darker sphere domain splits into two lighter spheres (highlighted in the dot circle in Fig. 7a). This indicates that the structure is composed of two layers of the hexagonal packed spheres, and they are completely superimposed on each other along the [111] zone, resulting in the darker color of the PDMS spheres. In contrast, there are some lighter PDMS spheres that are shown to be randomly packed instead of hexagonal packed. After being tilted in TEM, the neighboring spheres can be seen to overlap with each other to form a darker PDMS sphere (highlighted in the dot circle in Fig. 7b), indicating that two lighter PDMS spheres in the thin film are located incommensurately in different layers along the thin film normal, and they are not superimposed on each other.

Another interesting feature is the phase structures in the region where the thin film thickness changes. For example, after solvent vapor treatment for 12 hours (Fig. 6n), there are two different layer thicknesses, T_2 and T_3. Within these two layer thicknesses, their phase structures are identical as cylinders oriented parallel to the film substrate. In the T_2 layer, there are two layers of cylinders, and in the T_3 layer, there are three layers of cylinders.

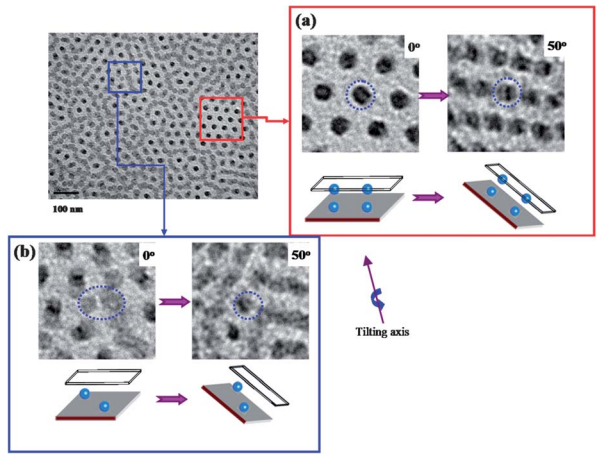

Fig. 7 TEM tilted images for the benzene annealed PS-*b*-PDMS thin film with a thickness around 56 nm.

However, in the region between the T_2 and T_3 layers where the film thickness continuously changes, Fig. 8 exhibits PDMS spheres, as proved by the tilted TEM observations illustrated in this figure. The general prediction for the stable structure in this region where the thicknesses change occurs is a cylinder, with the cylinder axis perpendicular to the thin film substrate.[9,14,44] This is because when the film thickness significantly deviates from an integer-multiple of the layer thickness, the blocks are supposedly not stretched or compressed if the cylinder axis is perpendicular to the thin film substrate; however they are stretched to a certain degree as the axis is parallel to the thin film substrate which is energetically unfavorable.[47] However, in our benzene vapor treated thin film, the region where the thickness changes between the T_2 and T_3 layers shows the spherical structure in Fig. 8 rather than the predicted cylinder structure. This indicates that the spherical structure in this series of PS-*b*-PDMS benzene vapor treated thin films has a free energy that is very close to the cylindrical structure and can be stabilized in this intermediate thickness region rather than return to its thermodynamic equilibrium structure.

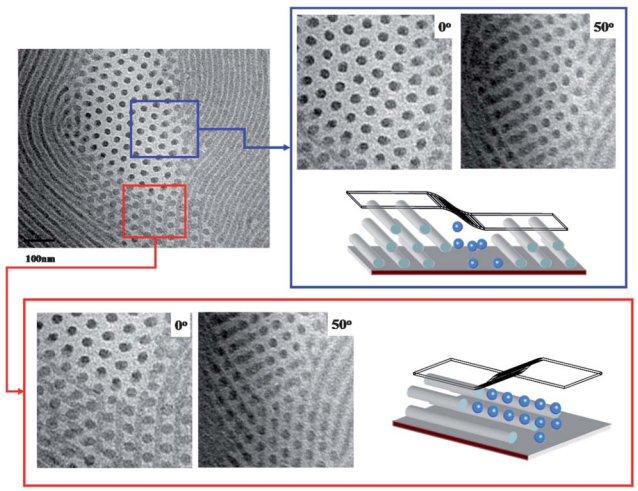

Fig. 8 TEM tilted images for the benzene annealed PS-*b*-PDMS thin film in the transition region between T_2 and T_3 layers.

This oscillating structural transition has not only been observed in benzene vapor treated samples but seems to be a general phenomenon when the PS-*b*-PDMS thin films are treated with a PS-selective solvent. Fig. 9 shows two sets of bright-field TEM images of the PS-*b*-PDMS thin film with an initial thickness of ~30 nm treated under controlled tetrahydrofuran (THF) solvent vapor. Compared to benzene solvent, THF has a similar solubility parameter ($\delta_{THF} \sim 18.6$ (J cm^{-3})$^{1/2}$) but a higher vapor pressure at room temperature, so the solvent concentration in the THF-treated thin film should be higher than the benzene-treated sample when the solvent treatment conditions are the same. During THF solvent vapor treatment, the oscillating structural transition in the thinner T_1 layer happens more frequently compared with those samples treated in benzene vapor (Fig. 9a–e). In the T_2 layer, instead of the oscillation between cylinders and spheres, it exhibits the oscillating structural transition between cylinders and cylinders combined with spheres or short rods (Fig. 9f–j). During the THF solvent vapor treatment, this oscillation of structural transition continuously occurs both in the T_1 and T_2 layers within the treated time studied.

However, different results were obtained when toluene solvent vapor ($\delta_{toluene} \sim 18.2$ (J cm^{-3})$^{1/2}$) was used, which is another common PS-selective solvent with a lower vapor pressure at room temperature. Fig. 10 shows a set of bright-field TEM images of toluene solvent vapor treated thin film samples. Unlike the other two sets of solvent treated thin film samples, during toluene solvent vapor treatment, there are neither any large grains of uniform structural transformation nor terrace formation before solvent treatment time of 6 hours. Similar to the thermally annealed samples shown in Fig. 3, the spherical structure was retained at the early stages of toluene solvent vapor treatment (Fig. 10a and d). The formation of cylinders only appears in small and local areas. Thin films then form islands and holes as the toluene solvent vapor treated time reaches 10 hours and an illustration of the film surface structure is shown in Fig. 10b. Fig. 10e shows the corresponding bright-field TEM images for the thin film with toluene solvent vapor treatment of 10 hours. In the holes and islands, which are marked as T_1 and T_3 in Fig. 10b and e, thin films show the cylindrical structure, and in the T_2 layer which has the thickness similar to the initial film thickness, the spherical structure is still retained. As the toluene vapor treated time increases, the area of the T_2 layer in Fig. 10b gradually shrinks and finally becomes the thickness transition region between the T_1 (with one layer of cylinders) and the T_3 (with two layers of cylinders) layers. The illustration of the thin film surface structure is shown in Fig. 10c, and its corresponding bright-field TEM images are shown in Fig. 10f. During a prolonged time toluene vapor treatment, we still can observe the oscillation of structural transition between the spheres and cylinders, but due to the slow kinetics and low vapor pressure that toluene provided, the structural transition we observed is only restricted to a local area with slow transition kinetics.

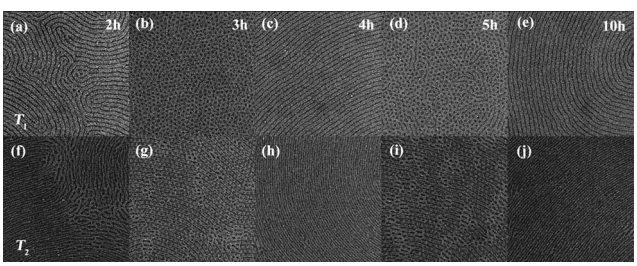

Fig. 9 Thin film structural transition during THF solvent annealing (film thickness ~ 30 nm). Each image is about 1 μm × 1 μm.

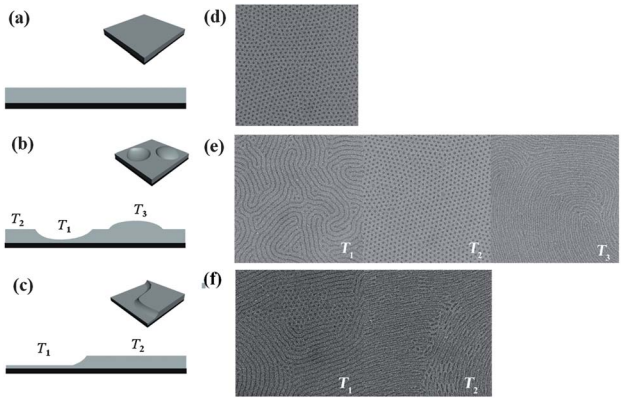

Fig. 10 Thin film structural transition during toluene vapor treatment (film thickness ~ 30 nm). (a–c) Illustration of film surfaces and cross-section evolution during toluene vapor treatment. Solvent treatment times of (a) 1–6 hours, (b) 6–10 hours, and (c) 14 hours. (d–f) The corresponding TEM bright images. Each image is about 1 μm × 1 μm.

Mechanism of ordering

Based on the observations described so far, we infer that in this PS-*b*-PDMS thin film system under the environment of utilizing PS-selective solvent vapor treatments, the vapor tends to swell the PS phase more than the PDMS phase and causes the PS volume fraction to increase and push the system composition towards the spherical side of the phase boundary between the cylinder and sphere phases. The free energies and transition barriers between the cylinder and sphere phases are relatively close to each other near the phase boundary. If we look at thin film morphology transition under benzene vapor treatment, we can find that thin film morphology transfers from PGMEA trapped spheres to cylinders after benzene vapor treatments for 2 hours, but at that time, the cylinder morphology is less ordered with a smaller grain size and a higher defect density. These defects can cause the increase of the free energy barrier for this cylinder phase to further transfer to the cylinder phase with a larger grain size and a lower defect density. To further follow the free energy pathway to achieve this thermodynamically more stable cylindrical phase, the existing solvent molecules within the thin film reduce the energy barrier for phase transition and increase the fluctuation of the system composition. The thermodynamic barriers for transitioning back to spheres are low enough that they provide a pathway to refine the spheres under a constant solvent concentration. According to the Gibbs Phase rule, the addition of the solvent to the system increases the degrees of freedom of the system, meaning that a window of phase coexistence could occur.[48] According to the data shown above, in this PS-*b*-PDMS thin film system the sphere and cylinder phases' co-existence is not thermodynamically favored

as the thin film morphology ultimately transitions to cylinders. But in the intermediate state, the free energy difference between a mixture of spheres and cylinders and high defect density cylindrical grains may be small, allowing for an oscillating transition. The structural defects, such as the grain boundaries between two mis-oriented cylinder domains, can thus serve as nucleation sites for further growing cylinders.[49,50] One possible transition pathway is to realign one cylinder grain with another. It is likely a very slow process that is kinetically unfavourable with a large thermodynamic barrier. Another accepted transition pathway is to break-up the cylinders back to spheres and then reform the cylinders, which is already known as an epitaxial growth process.[18,51,52] After the PDMS sphere phase forms, they can further connect with neighboring domains to construct cylinders with the correct orientation of the cylindrical nucleus to achieve a larger grain and a lower defect density. The grain size of the cylinder phase increases as this oscillating transition proceeds. According to the Gibbs–Thomson effect, with increasing area, the interfacial area and thus the interfacial tension decrease,[49,53] and the overall cylinder phase becomes increasingly stable. Finally, the thin film morphology is stabilized in this long-range ordering cylinder phase.

The kinetics of this oscillating structural transition are closely associated with the transient amount of solvent vapor absorbed by the PS blocks during the solvent vapor treatment process, where this absorption of the solvent vapor is critically associated with the solvent vapor pressure. The vapor pressure for THF is higher than that of benzene at room temperature, thus the PS phase volume fraction change in THF vapor pressure towards a higher value becomes faster than that in benzene vapor. In other words, the kinetics of the structural transition between spherical and cylindrical structures is quicker during the THF solvent vapor treatment comparing to that in the benzene solvent treatment. Therefore, the oscillating structural transition appears more frequently in THF solvent vapor treatment samples. In the contrast, toluene has the lowest vapor pressure at room temperature among these three solvents used. The toluene solvent vapor provided during the solvent treatment is not sufficient for the thin films to access the structural transition from the spherical structure to cylindrical structure in a time shorter than 6 hours. As the treatment time was prolonged, the oscillation between the two phase structures can still be found within each layer but this oscillated structural transformation occurs less frequently and is restricted to local areas. Comparing these observations in the solvent vapor treatment to the case in the thermal annealing where the thin film is stabilized in a locally trapped metastable state with a high energy barrier of the transition, the solvent vapor treatment leads to a decrease of this energy barrier for the structural transition, yet the volume fraction fluctuates in a large enough scale to give rise to the structural oscillation. This occurs even under the toluene solvent vapor treatment that possesses low vapor pressure. Therefore, it can be expected that this oscillation between two phase structures is a nucleation-controlled process.

Conclusions

In summary, a solvent induced spherical phase structure can be obtained in both thin and thick films by preparing a PS-*b*-PDMS thin film from PGMEA solution. This spherical structure is stabilized during thermal annealing by the high χ value between the PS and PDMS blocks which inhibit the structural transition even at 80 °C higher than the T_g^{PS}. Compared to the thermal annealing, the PS-*b*-PDMS thin film system shows an interesting and unique oscillation between spheres and cylinders under the solvent vapor treatment before the thin film phase structure reaches its final thermodynamic equilibrium. This could represent evidence of a unique thermodynamic pathway for re-orienting and ordering the cylindrical phase to achieve a larger grain size and lower defect density, where the metastable sphere domains are intermittently created to refine defects in the morphology.

References

1 M. A. Chavis, E. L. Schwartz and C. K. Ober, in *Complex Macromolecular Architectures*, John Wiley & Sons (Asia) Pte Ltd, 2011, pp. 763–790.
2 I. W. Hamley, *Prog. Polym. Sci.*, 2009, **34**, 1161–1210.
3 Y. Lei, S. Yang, M. Wu and G. Wilde, *Chem. Soc. Rev.*, 2011, **40**, 1247–1258.
4 C. Park, J. Yoon and E. L. Thomas, *Polymer*, 2003, **44**, 7779.
5 R. A. Segalman, *Mater. Sci. Eng., R*, 2005, **48**, 191–226.
6 M. Sommer, S. Huettner and M. Thelakkat, *J. Mater. Chem.*, 2010, **20**, 10788–10797.
7 J. N. L. Albert and T. H. Epps III, *Mater. Today*, 2010, **13**, 24–33.
8 T. P. Lodge, B. Pudil and K. J. Hanley, *Macromolecules*, 2002, **35**, 4707–4717.
9 A. Knoll, A. Horvat, K. S. Lyakhova, G. Krausch, G. J. A. Sevink, A. V. Zvelindovsky and R. Magerle, *Phys. Rev. Lett.*, 2002, **89**, 035501.
10 Z. Y. Di, D. Posselt, D. M. Smilgies and C. M. Papadakis, *Macromolecules*, 2010, **43**, 418–427.
11 M. Leolukman, Y. H. La, X. F. Li and P. Gopalan, *Polym. J.*, 2008, **40**, 825–831.
12 M. Y. Paik, J. K. Bosworth, D. M. Smilges, E. L. Schwartz, X. Andre and C. K. Ober, *Macromolecules*, 2010, **43**, 4253–4260.
13 J. Peng, Y. Xuan, H. F. Wang, Y. M. Yang, B. Y. Li and Y. C. Han, *J. Chem. Phys.*, 2004, **120**, 11163–11170.
14 A. Horvat, K. S. Lyakhova, G. J. A. Sevink, A. V. Zvelindovsky and R. Magerle, *J. Chem. Phys.*, 2004, **120**, 1117–1126.
15 K. S. Lyakhova, G. J. A. Sevink, A. V. Zvelindovsky, A. Horvat and R. Magerle, *J. Chem. Phys.*, 2004, **120**, 1127–1137.
16 Y. Wang, X. D. Hong, B. Q. Liu, C. Y. Ma and C. F. Zhang, *Macromolecules*, 2008, **41**, 5799–5808.
17 C. Y. Ryu and T. P. Lodge, *Macromolecules*, 1999, **32**, 7190–7201.
18 C. Y. Ryu, M. E. Vigild and T. P. Lodge, *Phys. Rev. Lett.*, 1998, **81**, 5354–5357.
19 S. Sakurai, T. Hashimoto and L. J. Fetters, *Macromolecules*, 1996, **29**, 740–747.
20 S. Sakurai, H. Kawada, T. Hashimoto and L. J. Fetters, *Macromolecules*, 1993, **26**, 5796–5802.
21 M. A. Modi, R. Krishnamoorti, M. F. Tse and H. C. Wang, *Macromolecules*, 1999, **32**, 4088–4097.
22 K. Kimishima, T. Koga and T. Hashimoto, *Macromolecules*, 2000, **33**, 968–977.
23 R. Krishnamoorti, M. A. Modi, M. F. Tse and H. C. Wang, *Macromolecules*, 2000, **33**, 3810–3817.
24 R. Krishnamoorti, A. S. Silva, M. A. Modi and B. Hammouda, *Macromolecules*, 2000, **33**, 3803–3809.
25 M. Li, Y. Liu, H. Nie, R. Bansil and M. Steinhart, *Macromolecules*, 2007, **40**, 9491–9502.
26 L. Tsarkova, A. Knoll and R. Magerle, *Nano Lett.*, 2006, **6**, 1574–1577.
27 A. Horvat, G. J. A. Sevink, A. V. Zvelindovsky, A. Krekhov and L. Tsarkova, *ACS Nano*, 2008, **2**, 1143–1152.
28 K. S. Lyakhova, A. V. Zvelindovsky and G. J. A. Sevink, *Macromolecules*, 2006, **39**, 3024–3037.
29 T. Xu, A. V. Zvelindovsky, G. J. A. Sevink, K. S. Lyakhova, H. Jinnai and T. P. Russell, *Macromolecules*, 2005, **38**, 10788–10798.

30 T. H. Kim, J. Huh, J. Hwang, H. C. Kim, S. H. Kim, B. H. Sohn and C. Park, *Macromolecules*, 2009, **42**, 6688–6697.
31 C. Y. Chang, P. J. Wu and Y. S. Sun, *Soft Matter*, 2011, **7**, 9140–9147.
32 Z. Wang, B. H. Li, Q. H. Jin, D. T. Ding and A. C. Shi, *Macromol. Theory Simul.*, 2008, **17**, 301–312.
33 Y. S. Jung and C. A. Ross, *Small*, 2009, **5**, 1654–1659.
34 T. Nose, *Polymer*, 1995, **36**, 2243–2248.
35 H. Frielinghaus, N. Hermsdorf, K. Almdal, K. Mortensen, L. Messe, L. Corvazier, J. P. A. Fairclough, A. J. Ryan, P. D. Olmsted and I. W. Hamley, *Europhys. Lett.*, 2001, **53**, 680–686.
36 N. J. Chou, C. H. Tang, J. Paraszczak and E. Babich, *Appl. Phys. Lett.*, 1985, **46**, 31–33.
37 M. A. Hartney, J. N. Chiang, D. W. Hess and D. S. Soane, *Appl. Phys. Lett.*, 1989, **54**, 1510–1512.
38 L. Li and H. Yokoyama, *Angew. Chem., Int. Ed.*, 2006, **45**, 6338–6341.
39 C. C. Chao, T. C. Wang, R. M. Ho, P. Georgopanos, A. Avgeropoulos and E. L. Thomas, *ACS Nano*, 2010, **4**, 2088–2094.
40 D. J. Kinning and E. L. Thomas, *Macromolecules*, 1984, **17**, 1712–1718.
41 K. J. Hanley, T. P. Lodge and C. I. Huang, *Macromolecules*, 2000, **33**, 5918–5931.
42 S. Z. D. Cheng, *Phase Transitions in Polymers: the Role of Metastable States*, Elsevier Science, 2008.
43 K. A. Cavicchi and T. P. Russell, *Macromolecules*, 2007, **40**, 1181–1186.
44 A. Knoll, R. Magerle and G. Krausch, *J. Chem. Phys.*, 2004, **120**, 1105–1116.
45 J. H. Chen, A. Q. Zhang, M. A. Yandrasites, S. Z. D. Cheng and V. Percec, *Makromol. Chem.*, 1993, **194**, 3135–3148.
46 S. D. Hudson and E. L. Thomas, *Phys. Rev. Lett.*, 1989, **62**, 1993–1996.
47 D. G. Walton, G. J. Kellogg, A. M. Mayes, P. Lambooy and T. P. Russell, *Macromolecules*, 1994, **27**, 6225–6228.
48 T. A. Mykhaylyk, S. Collins, I. W. Hamley, S. D. Evans and J. R. Henderson, *J. Mater. Sci.*, 2004, **39**, 2249–2252.
49 A. Knoll, K. S. Lyakhova, A. Horvat, G. Krausch, G. J. A. Sevink, A. V. Zvelindovsky and R. Magerle, *Nat. Mater.*, 2004, **3**, 886–890.
50 N. Sota and T. Hashimoto, *Polymer*, 2005, **46**, 10392–10404.
51 M. J. Park, J. Bang, T. Harada, K. Char and T. P. Lodge, *Macromolecules*, 2004, **37**, 9064–9075.
52 M. J. Park and K. Char, *Langmuir*, 2005, **21**, 1403–1411.
53 M. Perez, *Scr. Mater.*, 2005, **52**, 709–712.

Addition and correction

Note from RSC Publishing

This article was originally published with incorrect page numbers. This is the corrected, final version.

The Royal Society of Chemistry apologises for these errors and any consequent inconvenience to authors and readers.